Impact of lattice inclusion of Cu and Fe ions on thermal decomposition characteristics of ammonium perchlorate

Savitha Nair[1], Suresh Mathew[2] and Reghunadhan C.P. Nair[3]

[1] Vikram Sarabhai Space Centre, Thiruvananthapuram, Kerala, India
[2] School of Chemical Science, Mahatma Gandhi University, Kottayam, Kerala, India
[3] Cochin University of Science and Technology, Ernakulam, Kerala, India

ABSTRACT

Ammonium perchlorate (AP) is the universal oxidiser in use for all the solid rocket propellant motors used for space exploration due to its high available oxygen content and thermal decomposition without any solid residue. The inclusion of reactive species in AP directly affect the viscoelastic and ballistic properties of the propellant. Variations in lattice configuration of AP change its physical and thermal characteristics dramatically. In the present work AP was doped with Copper perchlorate and Iron perchlorate through co crystallisation. The impact of inclusion of these ionic species in the lattice on the thermal decomposition characteristics of AP was examined. The incorporation affected the physical as well as the ballistic characteristics of the resultant AP. The incorporation of foreign ions into AP crystals significantly changed the crystal morphology. The decomposition temperature decreased vis-a-vis with normal AP. The activation energy remarkably decreased for the doped AP crystals.

INTRODUCTION

The important chemical formulation used in rocketry is Composite Solid Propellant (CSP). CSP gives driving force to the rocket. Its important parameters are thermal stability, burning rate, friction and impact sensitivity. AP used as oxidiser is the major component (about 70%) in CSP. Thermal decomposition of AP directly influences the combustion behaviour of the propellant. The reduction in particle size of AP or metallic fuel may increase the burning surface area which in turn increases the burn rate of a propellant. The high thrust requirement of missions are satisfied by either increasing the burning surface area or by the addition of burn rate modifiers (BRM). The commonly used BRM are iron oxide and copper chromite (<3%). The doping of AP with transition metals and their oxides has shown to decrease the activation energy and decomposition temperature of AP, thereby acting as good catalysts (*Schumacher, 1960*; *Boldyrev, 2006*; *Jacobs & Whitehead, 1969*; *Kishore & Sunitha, 1979*). The mechanical mixing of AP with compounds of copper and iron is highly effective in reducing the thermal decomposition of Ammonium perchlorate (*Wang et al., 2013*; *Patil, Krishnamurthy & Joshi, 2008*;

Chen, Li & Li, 2008b, *2008a*; *Alizadeh-Gheshlaghi et al., 2012*; *Yang et al., 2014*; *Liu et al., 2004*; *Chaturvedi & Dave, 2013*; *Styborski et al., 2015*; *Song et al., 2010*; *Costa et al., 2009*).

The crystallization being the critical step in the manufacturing of AP, the modifications made in crystallization parameters alter the crystal strength, purity and particle size distribution of AP (*Mullin, 1997*; *Lakshmi et al., 2016*). Previous works have reported the inclusion of foreign metal ions into AP crystal and its impact on the thermal decomposition characteristics; but the physical and crystallographic aspects were not discussed (*Boldyrev, 2006*; *Jacobs & Whitehead, 1969*; *Pelly, 1982*). The addition of BRM to AP can be done by either physical mixing or by co-crystallisation. The co-crystallisation of AP with salts results in the lattice inclusion of compounds into AP lattice. Variations in lattice configuration of AP changes its physical, thermal and ballistic characteristics dramatically, while the basic thermodynamic properties could remain unaltered.
The present work focus on the alteration in lattice configuration of AP by co-crystallisation with perchlorates of copper and iron. The doped AP crystals were analysed for studying the impact of lattice inclusion of Cu and Fe ions on the lattice, physical and thermal characteristics of AP. The incorporation of foreign ions into AP crystals significantly changed the crystal morphology, bulk density, moisture content and the decomposition behaviour compared with normal AP. The decomposition temperature and activation energy remarkably decreased for the doped AP crystals.

EXPERIMENTAL

Materials

Ammonium perchlorate crystals of purity >99.0% processed at Ammonium Perchlorate Experimental Plant, Aluva, Kerala was used for the preparation of doped AP in the present work. Analytical grade reagent copper perchlorate hexahydrate, and ferrous perchlorate nonhydrate from MERCK was used as received for doping of AP.

Co-crystallization

A glass jacketed crystallizer of 5L capacity with glass agitator and teflon paddle is used for crystallization. The super saturated solution of AP was prepared in distilled water at 75 °C, and the secondary nucleation was prevented by increasing the temperature of the solution by 5 °C. The separation of AP crystals from solution was done by cooling crystallisation method owing to the high temperature coefficient of solubility for AP. The concentration of copper perchlorate/iron perchlorate in mother liquor was varied from 10% to 20% by weight of AP. While the rpm of the agitator was set at slow rate that is 50 rpm; a fast cooling mode of 0.6 °C/min was used to get doped crystal of substantial crystal properties and concentration. The crystallisation condition optimisation was done through a number of experimental trials and statistical calculation (*Nair, Mathew & Reghunadhan Nair, 2020*; *Nair et al., 2020*). Two different concentrations each of copper doped AP and iron doped AP were prepared. Copper doped AP was prepared by co-crystallisation of AP with copper perchlorate, and iron doped AP was prepared by co-crystallisation of AP with iron perchlorate. The doped samples were named

ACuP-1 (Cu-0.36%), ACuP-2 (Cu-0.49%), AFeP-1 (Fe-0.35%), and AFeP-2 (Fe-0.51%) respectively. The prepared doped AP crystals were filtered out and dried in glass trays and dried at 60 °C for 4 h in laboratory hot air oven.

Instrumentation

The particle size distribution (PSD) of the doped AP was measured by sieve analysis method using Ro-Tap sieve shaker. The weighted average particle size was calculated by sieve analysis, using sieves of size 45–500 μm. The copper and iron content in the doped AP crystals were measured using ICP-AES. The specific surface areas of the particles were measured by multipoint BET method using Quantachrome NOVA 1200e Surface Area Analyzer. The friability of AP crystals were measured using crystals of particle size >125 μm. The crystals were given rotation and gyration for 30 min along with 100 numbers of 3 mm glass beads. The percentage weight loss is measured as the friability of the crystals. The bulk density measurement was done with DBK bulk density apparatus having 100 ml measuring cylinder for filling the AP crystals. The volume change after 100 tapping is used for bulk density calculation. IR Moisture Analyser is used for the estimation moisture content in the sample. Field emission scanning electron microscopy (FESEM) observations were performed to examine the morphology of the samples using Carl Zeiss, Supra 55 model field emission scanning electron microscope. The crystallographic properties of AP samples were examined by collecting the powder X-ray diffraction data of the samples on a Bruker D8-Discover powder X-ray diffractometer with Cu Kα (λ = 1.5418 Å) at a scan rate of 2.5 deg per min. Static and Dynamic imaging techniques were performed to study the crystal characteristics. The Ankersmid Eyetech particle size and shape analyser measured the shape factor of the crystals. Perkin Elmer Simultaneous Thermogravimetry–Differential Scanning Calorimetry (TG-DSC), TA Instruments Q600, was employed for thermal characterisation. The thermal analysis was done at three different heating rates—3 °C/min, 5 °C/min and 10 °C/min—and kinetic analysis was done by Flynn–Wall–Ozawa Method (FWO).

RESULTS AND DISCUSSIONS

Physical characteristics

The dopants present in the mother liquor affect the crystal formation, and growth of the crystal. The crystal growth was inhibited slightly by the presence of dopant ion which results in decrease in particle size. The weight average particle size of normal AP is 312 μm. The average particle size of copper doped and iron doped AP is found to be 284 μm and 292 μm respectively. The dopant ion inclusion in AP lattice resulted in point defects, and the strength of the crystals got reduced. The reduction in strength of crystal increases the friability of the crystal. The friability of copper/iron doped AP crystals were found to be 0.72% and 0.71% respectively, slightly higher than friability of normal AP 0.68%. The specific surface area of normal and doped AP crystals were measured using multipoint BET and it is in the range 0.17–0.19 m²/g for normal AP and 0.22–0.24 m²/g for copper/iron doped AP. The surface roughness of doped crystals increases the surface area. The reduction in particle size with doping is a factor for increasing the surface area, and

Table 1 Physical characteristics of normal and doped AP.

Sample ref.	Weight % of Cu/Fe	Mole % of Cu/Fe	Average particle size (μm)	Friability (%)	Bulk density	Moisture (%)	Specific surface area (m/g)
AP	0	0	312	0.68	1.30	0.10	0.18
ACuP-1	0.36	0.007	291	0.71	1.28	0.13	0.22
ACuP-2	0.49	0.009	284	0.72	1.27	0.16	0.22
AFeP-1	0.35	0.007	296	0.70	1.33	0.12	0.24
AFeP-2	0.51	0.01	292	0.71	1.33	0.15	0.24
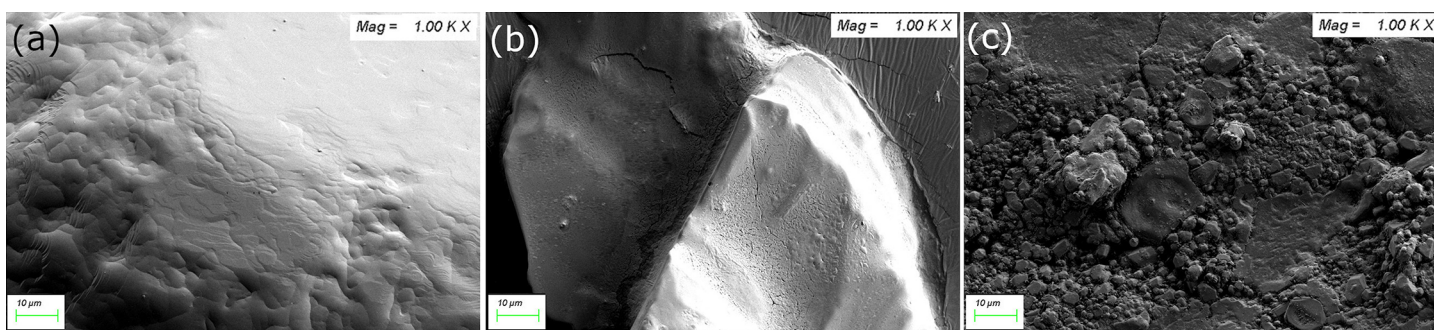
Figure 1 SEM images of (A) Normal AP, (B) ACuP-2, and (C) AFeP-2. Full-size 🖼 DOI: 10.7717/peerj-ichem.1/fig-1

bulk density. The bulk density usually increases with decrease in the particle size of the material, due to better packing and compactness for smaller particles and reduction in the number of voids or pores. Thus the doped AP is a better option to increase the compactness of the particle during propellant mixing. The moisture content increases with increase in dopant concentration, it is within allowed limits for propellant grade AP. For propellant grade AP the maximum allowed moisture content is 0.25%, for copper doped AP it is 0.16% and for iron doped AP it is 0.15%. The physical characteristics of normal and doped AP are given in Table 1.

The crystal surface morphology for normal AP and doped AP samples were studied by taking the scanning electron microscopy image of a single particle. Figures 1A–1C show the SEM images of normal AP, ACuP-2 and AFeP-2. The regularity and spherical nature of the particles get worsened by doping with copper/iron perchlorate due to the fast cooling mode. The SEM results show homogeneous doping of copper/iron perchlorate. Since the particles are of average particle size ~300 μm, the SEM image with high resolution (magnification 1,000×) were taken to cover the surface image of the particles for checking the homogeneity of doping. The doped crystals have more needle like crystal growth compared with normal AP.

The elemental mapping of the doped crystal was conducted to check the uniform distribution of Copper/Iron in the crystals. The images in Fig. 2 give the clear idea that the dopant ions are uniformly distributed throughout the AP crystal. Since the stability of the
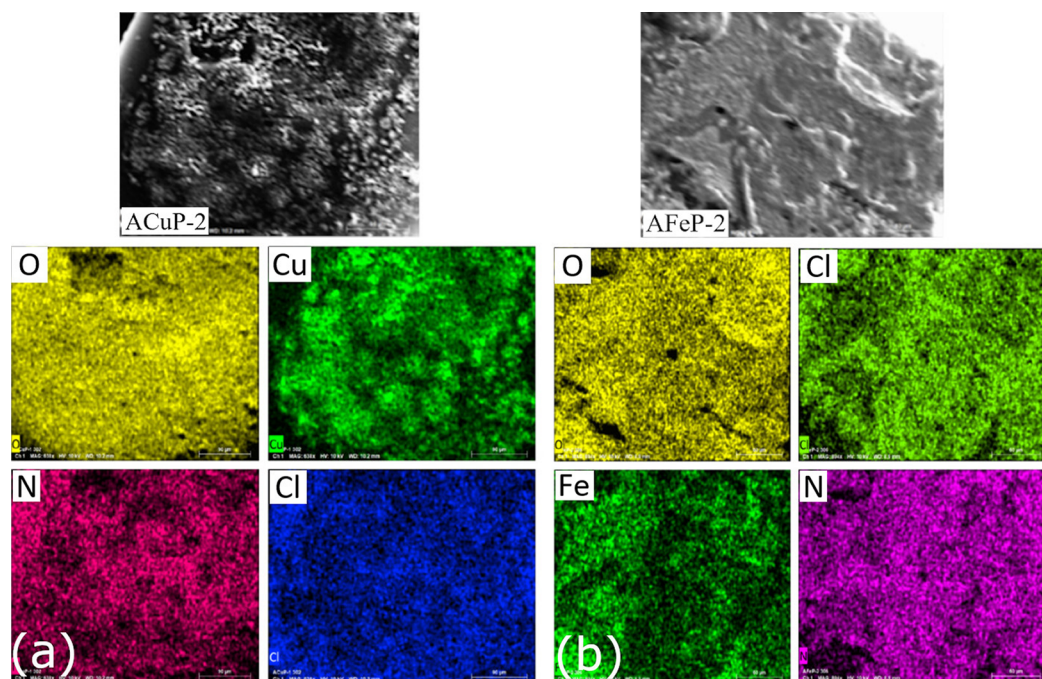
Figure 2 Elemental mapping of (A) ACuP-2 and (B) AFeP-2.
Full-size ☒ DOI: 10.7717/peerj-ichem.1/fig-2

ionic co-crystal formed is less than those of pure AP, the EDS spectra showed separation of elements when compared to other compounds.

Crystallographic characteristics

The XRD patterns of the standard AP samples were given by the JCPDS pattern with reference code: 000080451. The major peaks appear for AP crystals were at 2θ values of 15.3°, 19.4°, 22.7°, 23.9°, 24.6°, 27.4°, 30.1°, 30.8° and 34.6° assigned to the (101), (011), (201), (002), (210), (211), (112), (202) and (212) crystal planes respectively. Figure 3 compares the XRD peaks of normal AP and the AP doped with copper and iron perchlorate respectively. The needle like growth of the crystals resulted in reduction in number of peaks in the XRD pattern. For ACuP-2, the relative intensity at 23.9° was remarkably high, and only two peaks—23.9 and 30.1—are present. For iron doped AP, the peak at 24.6 got intensified. It shows that the doping of AP crystal with copper perchlorate and iron perchlorate have a crystal habit modification effect on AP.

The interpretation of XRD data for details related to spacing between the lattice planes and shape of the crystal lattice were done using Bragg's law. The Bragg's law relates the distance between lattice planes d, wavelength of radiation λ, and the diffraction angle θ, as $2d\sin\theta = n\lambda$.

Due to co-crystallisation the spacing between atoms in the crystal increases, the 2θ angle vary, resulting in a shorter path length for the X-rays to interfere constructively. According to Bragg's law, the spacing between planes d, and by extension the lattice parameters must then increase to compensate for the reduction of θ, as λ is not changing. The doping of AP with metal ions resulted in the expanding d distance between lattice planes.
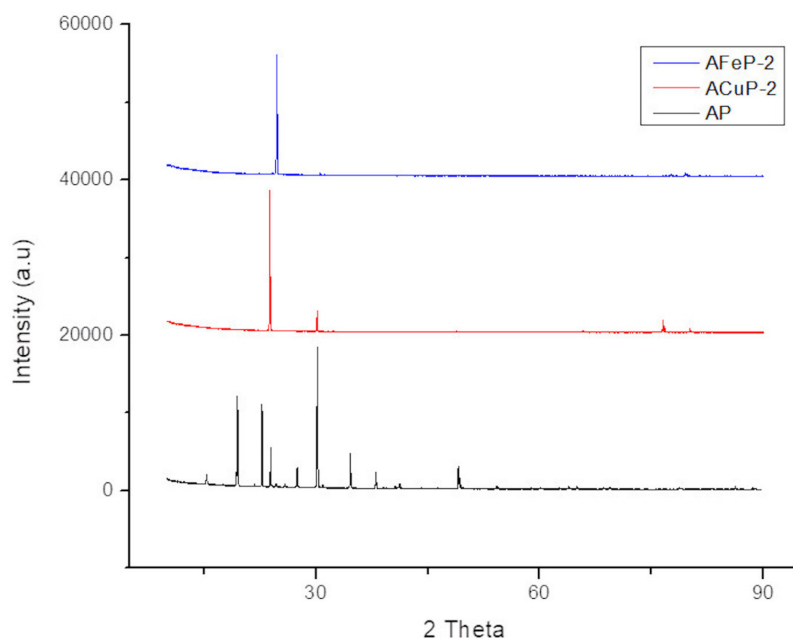
Figure 3 XRD pattern of normal AP, ACuP-2 and AFeP-2.
Full-size ◩ DOI: 10.7717/peerj-ichem.1/fig-3

Table 2 Lattice parameters and lattice volume of AP, ACuP-2 and AFeP-2.

Sl. no.	Sample ref.	a (nm)	b (nm)	c (nm)	V (nm^3)
	AP	0.9169	0.5824	0.7424	0.3964
	ACuP-2	0.9172	0.5797	0.7427	0.3949
	AFeP-2	0.8928	0.6238	0.7609	0.4238

The AP crystals were existing in an orthorhombic shape requiring the need to determine the lattice parameters *a*, *b*, and *c*. Boldyrev reports these lattice parameters as 0.9202, 0.5816, and 0.7449 nm for *a*, *b*, and *c*, respectively (*Boldyrev, 2006*). Choosing *h*, *k*, and *l* values along with using the cited lattice parameters allows for the generation of approximate 2θ values associated with the chosen Miller index. The estimation of peak locations were done using Equation 1 $d^2 = h^2 a^2 k^2 b^2 \frac{l^2}{c^2}$.

So the peaks of (201), (002), and (210) were selected to solve for lattice parameters *a*, *b*, and *c* for each samples. The lattice parameters determined were shown in the Table 2. The inclusion of copper ion into AP lattice increased lattice parameter *a* and *c* slightly, and reduced lattice parameter *b*. For AFeP-2, the cation inclusion reduced the lattice parameter *a*, and increased lattice parameter *b* and *c*, resulting in a substantial increase in the lattice volume. This shows that the inclusion of cations into AP lattice causes distortion of the orthorhombic structure. This strained state increases the enthalpy of the system thus bringing down the numerical value of the free energy change (ΔG).
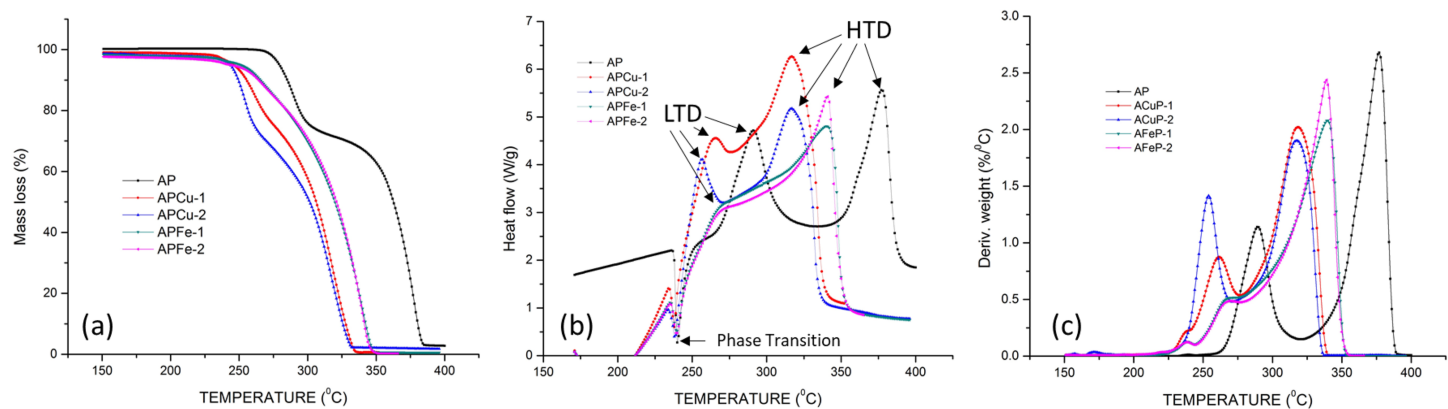
Figure 4 (A) TGA curve of AP and doped AP (ACuP-1, ACuP-2, AFeP-1, AFeP-2), (B) DSC curve of AP and (ACuP-1, ACuP-2, AFeP-1, AFeP-2) and (C) DTG curve of AP and (ACuP-1, ACuP-2, AFeP-1, AFeP-2). Full-size ⊠ DOI: 10.7717/peerj-ichem.1/fig-4

Table 3 Phenomenological data for the decomposition of normal AP and Doped AP.

| Sample ref.	Dopant conc. (%)	LTD				HTD			
		Ti	Tp	Tf	Mass-loss (%)	Ti	Tp	Tf	Mass-loss (%)
AP	0	244	285	312	30	312	374	388	70
ACuP-1	0.36	225	260	274	29	274	317	341	71
ACuP-2	0.49	211	253	269	29	269	314	336	71
AFeP-1	0.35	216	263	273	31	273	338	355	69
AFeP-2	0.51	213	262	270	31	270	337	353	69

Thermal characteristics

The Thermo Gravimetric (TG) and Differential Scanning Calorimetry (DSC) measurements were used to study the thermal characteristics of the normal AP and doped AP. The thermal decomposition of AP occurs in two-stages—the low temperature decomposition (LTD) starting at around 240 °C (accounting for 30% mass loss) is immediately followed by the second stage high temperature decomposition (HTD) that completes at around 380 °C. The crystallographic transition from orthorhombic to cubic form is given by the endotherm at 240 °C.

The overlaid TG curves of Cu/Fe doped AP and normal AP are shown in Fig. 4A. There is a substantial decrease in the decomposition temperature for LTD and HTD which shows the catalytic nature of Cu/Fe on thermal decomposition of AP. The phenomenological data for the thermal decomposition is shown in Table 3, and it shows that the thermal decomposition peaks completely shift to a lower regime and it was clear from the lowering of initial temperature (Ti), peak temperature (Tp) and final temperature (Tf) of LTD and HTD. The high catalytic activity of copper ion for the thermal decomposition of AP resulted in a lowering of LTD by 32 °C and HTD by 60 °C. However, the efficiency of iron in accelerating the thermal decomposition of AP is less compared to copper where the LTD decrease by 23 °C and the HTD by 37 °C. Moreover, the effect of change in copper concentration on thermal decomposition of AP is found

Table 4 Activation energy for thermal decomposition of AP, ACuP-2 and AFeP-2.

Sample ref.	E (kJ/mol)	
	LTD	HTD
Normal AP	149.2	123.2
ACuP-2	89.7	116.5
AFeP-2	137.1	122.5
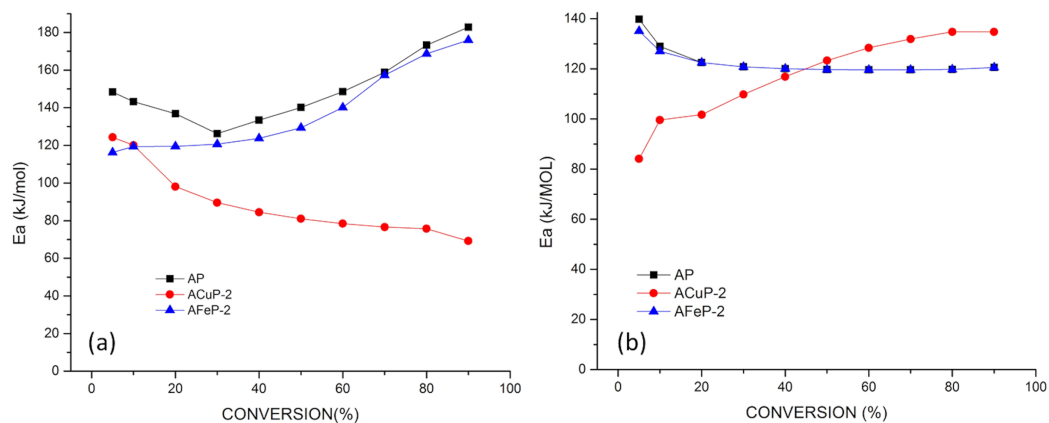
Figure 5 (A) Ea vs conversion plot for normal AP and doped AP: (A) LTD, (B) HTD.
Full-size ⬇ DOI: 10.7717/peerj-ichem.1/fig-5

to be more than that for iron. The change in iron concentration does not make much effect on the thermal decomposition and the peaks are found to be closer to each other, and the same can be realised from the data given in Table 3. The mass loss during thermal decomposition is slightly more for LTD of iron doped AP, and HTD of copper doped AP. It may be due to the conversion of copper to copper oxide during the thermal decomposition which further catalyses the reaction. The physical mixing of AP with compounds catalyse the HTD only. For the lattice modified AP, catalysing both the thermal decomposition stages result in a substantial increase in burn rate in AP containing propellant (*Dey et al., 2015*).

The DSC curve given by Fig. 4B shows the catalytic nature of copper and iron on thermal decomposition of AP, and the heat release for the doped samples were found to be higher than that of normal AP. The DTG curve shown in Fig. 4C clearly shows the shift in decomposition peaks.

The doped AP samples ACuP-2 and AFeP-2 were taken for kinetic analysis. For the calculation of activation energy by FWO method, the thermal analysis were done at three different heating rate 3 °C/min, 5 °C/min and 10 °C/min. The activation energy for these samples were less than that of normal AP samples and it is given in Table 4. The activation energy vs conversion plot is given in Fig. 5. There is a decrease in activation energy supporting the effectiveness of catalytic process. The kinetic analysis result shows a prominent decrease in the activation energy which indicates copper is a good catalyst compared to iron in this particular case.

$$NH_4^+ + ClO_4^- \quad \rightarrow \quad NH_3(a) + HClO_4(a) \quad \rightarrow \quad NH_3(g) + HClO_4(g)$$
$$\text{I} \qquad\qquad\qquad\qquad \text{II} \qquad\qquad\qquad\qquad\qquad \text{III}$$

Scheme 1 Thermal decomposition of AP.   Full-size 🖼 DOI: 10.7717/peerj-ichem.1/scheme-1

The experimental results on AP doped with Cu/Fe showed that the lattice modification was effective to reduce both the low temperature and high temperature decomposition. The solid phase reactions occurs only in LTD, while gas phase reactions occurs in both LTD and HTD. Earlier works on the thermal decomposition of AP proposed the electron transfer from ClO_4^- to NH_4^+ as the scheme of mechanism (Scheme 1) (*Boldyrev, 2006*; *Jacobs & Whitehead, 1969*; *Kishore & Sunitha, 1979*; *Wang et al., 2013*; *Patil, Krishnamurthy & Joshi, 2008*).

The NH_4^+ and ClO_4^- ions are formed in the lattice in first step, followed by proton transfer from ammonium ion (cation) to perchlorate ion (anion) via a molecular complex formation. The last step is decomposition proceeds to form ammonia and perchloric acid. The low temperature decomposition reactions start from the core and proceeds to the surface, often involve both bond-breaking and bond-forming steps.

The inclusion of copper ion and change in crystallisation parameters resulted in increased surface area of copper doped AP. The lattice included copper acts as the initiation point for the thermal decomposition it get oxidised to CuO due to the increased heat release during thermal decomposition of AP. The presence of ions of copper with two different valencies promote the electron transfer mechanism. The activation energy is found to be increased during LTD, which can be due to the conversion of Cu to CuO, after the complete conversion of CuO the activation energy is decreased. Positive holes in CuO can accept electrons and it act as a surface for high temperature decomposition.

In iron doped AP crystals, the surface area is found to be increased due to the porous nature of surface of the crystals. Iron content in the crystal promotes both low temperature and high temperature decompositions. The Fe^{2+}/Fe^{3+} transition facilitates the electron transfer mechanism. Since the metal ion is present in the lattice it can act as an initiation point for thermal decomposition to start. During thermal decomposition it is converted to Fe_2O_3 and favours HTD by acting as a catalytic surface. The doped iron converted to Fe_2O_3 increases the surface area and act as a surface for further thermal decomposition of AP as HTD is a surface phenomenon.

The catalytic activity can be attributed to the presence of Cu/Fe ions throughout the crystal lattice, as well as the synergetic effect of the oxides of copper/iron during the thermal decomposition of AP. The formation of cuprous/cupric oxides or ferrous/ferric oxides will enhance the redox reaction taking place during the decomposition of AP by acting as a better carrier or conductor of electrons.

CONCLUSION

The decomposition characteristics of AP crystals were improved by lattice modification with iron perchlorate and copper perchlorate. The inclusion of cations into AP lattice alter the lattice parameters resulting in more stress in the crystals, and hence it acts as a point

for the thermal decomposition initiation. The lattice modified AP crystal has better decomposition characteristics. The average particle size of copper/iron doped AP was decreased and an increase in friability and bulk density was observed. The inclusion of copper/iron perchlorate into AP lattice via co-crystallisation resulted in the production of AP with good particle size distribution and friability. The doped crystals with low decomposition temperature form the basis of its application as high burn rate propellant. Lattice inclusion of copper ion is found to be an efficient method for improving the thermal decomposition characteristics of AP, and in turn the ballistic properties of the propellant.

ACKNOWLEDGEMENTS

ADDITIONAL INFORMATION AND DECLARATIONS

Funding

Competing Interests

The authors declare that they have no competing interests.

Author Contributions

- Savitha Nair conceived and designed the experiments, performed the experiments, analysed the data, prepared figures and/or tables, authored or reviewed drafts of the paper, and approved the final draft.
- Suresh Mathew analysed the data, authored or reviewed drafts of the paper, and approved the final draft.
- Reghunadhan C.P. Nair conceived and designed the experiments, analysed the data, authored or reviewed drafts of the paper, and approved the final draft.

Data Availability

The following information was supplied regarding data availability:

Data are available as a Supplemental File.

Supplemental Information

Supplemental information for this article can be found online at http://dx.doi.org/10.7717/peerj-ichem.1#supplemental-information.

REFERENCES

Alizadeh-Gheshlaghi E, Shaabani B, Khodayari A, Azizian-Kalandaragh Y, Rahimi R. 2012. Investigation of the catalytic activity of nano-sized cuo, co3o4 and cuco2o4 powders on thermal decomposition of ammonium perchlorate. *Powder Technology* **217**:330–339 DOI 10.1016/j.powtec.2011.10.045.

Boldyrev V. 2006. Thermal decomposition of ammonium perchlorate. *Thermochimica Acta* **443(1)**:1–36 DOI 10.1016/j.tca.2005.11.038.

Chaturvedi S, Dave PN. 2013. A review on the use of nanometals as catalysts for the thermal decomposition of ammonium perchlorate. *Journal of Saudi Chemical Society* **17(2)**:135–149 DOI 10.1016/j.jscs.2011.05.009.

Chen L, Li L, Li G. 2008a. Synthesis of cuo nanorods and their catalytic activity in the thermal decomposition of ammonium perchlorate. *Journal of Alloys and Compounds* **464(1–2)**:532–536 DOI 10.1016/j.jallcom.2007.10.058.

Chen L-J, Li G-S, Li L-P. 2008b. Cuo nanocrystals in thermal decomposition of ammonium perchlorate. *Journal of Thermal Analysis and Calorimetry* **91(2)**:581–587 DOI 10.1007/s10973-007-8496-7.

Costa A, Silva V, Ferreira H, Costa A, Cornejo D, Kiminami R, Gama L. 2009. Structural and magnetic properties of chromium-doped ferrite nanopowders. *Journal of Alloys and Compounds* **483(1–2)**:655–657 DOI 10.1016/j.jallcom.2008.08.129.

Dey A, Athar J, Varma P, Prasant H, Sikder AK, Chattopadhyay S. 2015. Graphene-iron oxide nanocomposite (GINC): an efficient catalyst for ammonium perchlorate (AP) decomposition and burn rate enhancer for AP based composite propellant. *RSC Advances* **5(3)**:1950–1960 DOI 10.1039/C4RA10812D.

Jacobs PWM, Whitehead H. 1969. Decomposition and combustion of ammonium perchlorate. *Chemical Reviews* **69(4)**:551–590 DOI 10.1021/cr60260a005.

Kishore K, Sunitha M. 1979. Effect of transition metal oxides on decomposition and deflagration of composite solid propellant systems: a survey. *AIAA Journal* **17(10)**:1118–1125 DOI 10.2514/3.61286.

Lakshmi V, Chakravarthy S, Rajendran A, Thomas C. 2016. Effect of crystallization parameters and presence of surfactant on ammonium perchlorate crystal characteristics. *Particulate Science and Technology* **34(3)**:308–316 DOI 10.1080/02726351.2015.1076102.

Liu L, Li F, Tan L, Ming L, Yi Y. 2004. Effects of nanometer ni, cu, al and nicu powders on the thermal decomposition of ammonium perchlorate. *Propellants, Explosives, Pyrotechnics: An International Journal Dealing with Scientific and Technological Aspects of Energetic Materials* **29(1)**:34–38.

Mullin JW. 1997. *Crystallization.* Oxford: Butterworth-Heinemann.

Nair S, Mathew S, Reghunadhan Nair CP. 2020. Lattice inclusion of copper ions in ammonium perchlorate through co-crystallization: impact on lattice, physical, and thermal characteristics. *ACS Omega* **5(30)**:18544–18550 DOI 10.1021/acsomega.9b03893.

Nair S, Nair SK, Nair CR, Mathew S. 2020. Crystallization modelling for lattice modified ammonium perchlorate. *AIP Conference Proceedings* **2263**:040005.

Patil PR, Krishnamurthy VN, Joshi SS. 2008. Effect of nano-copper oxide and copper chromite on the thermal decomposition of ammonium perchlorate. *Propellants, Explosives, Pyrotechnics: An International Journal Dealing with Scientific and Technological Aspects of Energetic Materials* **33(4)**:266–270.

Pelly I. 1982. The thermal decomposition of doped ammonium perchlorate. *Thermochimica Acta* **55(1)**:27–34 DOI 10.1016/0040-6031(82)87004-4.

Schumacher JC. 1960. *Perchlorates: their properties, manufacture, and uses.* Vol. 146. New York: Reinhold Publishing Corporation.

Song L, Zhang S, Chen B, Ge J, Jia X. 2010. A hydrothermal method for preparation of α-fe2o3 nanotubes and their catalytic performance for thermal decomposition of ammonium

perchlorate. *Colloids and Surfaces A: Physicochemical and Engineering Aspects* **360(1–3)**:1–5 DOI 10.1016/j.colsurfa.2010.01.012.

Styborski JA, Scorza MJ, Smith MN, Oehlschlaeger MA. 2015. Iron nanoparticle additives as burning rate enhancers in ap/htpb composite propellants. *Propellants, Explosives, Pyrotechnics* **40(2)**:253–259 DOI 10.1002/prep.201400078.

Wang C, Zhang H, Ye Y, Shen R, Hu Y. 2013. Effect of nanostructured foamed porous copper on the thermal decomposition of ammonium perchlorate. *Thermochimica Acta* **568**:161–164 DOI 10.1016/j.tca.2013.06.035.

Yang C, Xiao F, Wang J, Su X. 2014. Synthesis and microwave modification of cuo nanoparticles: crystallinity and morphological variations, catalysis, and gas sensing. *Journal of Colloid and Interface Science* **435**:34–42 DOI 10.1016/j.jcis.2014.08.044.

Nair et al. (2020), *PeerJ Inorganic Chemistry*, DOI 10.7717/peerj-ichem.1

12/12